Off-Axis-NOTE-SIM-32
David A. Petyt
April 1, 2004

Other oscillation measurements in the off-axis detector

Abstract

In addition to searches for non-zero θ_{13}, the off-axis detector has the potential to significantly improve the measurement errors on the oscillation parameters Δm^2_{23} and θ_{23} from a precise measurement of the ν_μ CC energy spectrum, and also to improve limits on the admixture of sterile neutrinos over those expected from the first generation of long-baseline neutrino oscillation experiments. This note presents the results of preliminary simulations studies, showing the expected sensitivity of the off-axis detector to these oscillation signals.

1 Selection algorithm

The simulated events used in these analyses were generated assuming a scintillator-based detector and were weighted to correspond to the expected energy spectrum for a distance of 810 km from the neutrino source and 12 km off-axis. Details of the event generation and detector simulation can be found elsewhere [1]. An exposure corresponding to 250 kiloton years with a proton intensity of 3.7e20 p.o.t/yr. was assumed for all the results in this note.

Several discriminating variables were used in a likelihood-based analysis to separate neutral current and charged-current events. A likelihood analysis was used here since, for most variables, there is significant overlap between the NC and CC distributions in the energy region of interest (1-3 GeV). A Hough Transform was applied (using the same algorithm as was used for the ν_e analysis [1]) to identify and isolate track-like elements within events and additional variables were derived from these track-like hits to provide further discrimination between CC and NC events. The variables used were:

- **Basic quantities:** event length, number of planes, number of hits, summed pulse height, 2D plot of hits per plane versus pulse height per plane.
- **Quantities derived from hits selected by Hough Transform:** total pulse height, pulse height per plane, fraction of total hits contained in track, fraction of total pulse height contained in track, 2D plot of track angle with respect to Fermilab versus total pulse height.

Figure 1 shows the distributions of several of these quantities for true NC and CC events. These distributions were used as probability density functions in order to evaluate the likelihood that a given event was CC-like or NC-like. The likelihood was formed from the product of the individual probabilities and the ratio of CC-like and NC-like likelihoods was taken. The likelihood ratio distributions for true CC and NC events are shown in figure 2. Independent CC-like and NC-like samples were obtained by applying a cut to

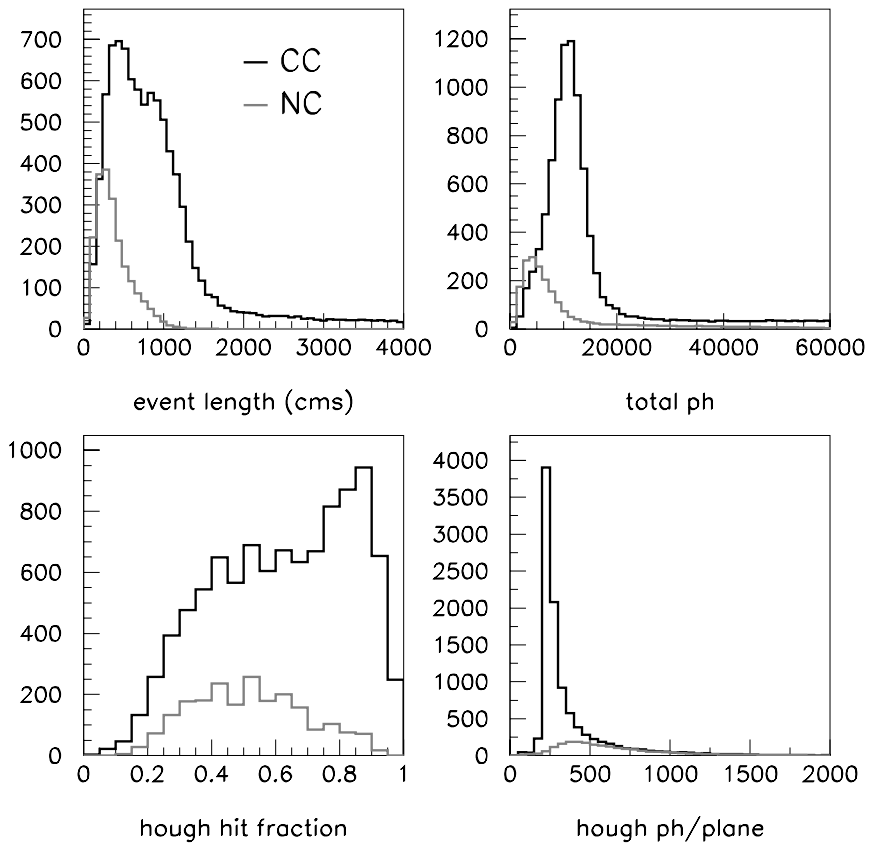

Figure 1: Distributions of quantities used to separate CC and NC events. Top-left: total event length (in cms); top-right: total summed pulse height (in photoelectrons); bottom-left: fraction of total hits found by the Hough Transform; bottom-right: pulse height per plane for hits found by the Hough Transform.

the likelihood ratio: a ratio greater than -1 defined CC-like events and a ratio less than -4 defined NC-like events. The CC-like sample has a selection efficiency of 82.4% for true charged-current events and a 7% contamination of NC events. The NC-like sample has a 58% selection efficiency for true NC events and a 42% contamination of mis-identified CC events.

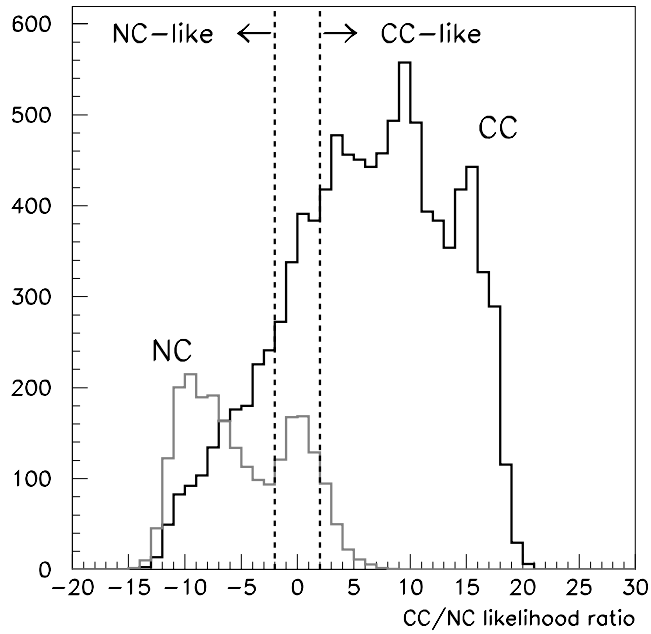

Figure 2: Likelihood ratio distributions for true CC and NC events. The cuts used to define CC-like and NC-like samples are indicated by the two dashed lines.

2 ν_μ disappearance measurements

The CC-like events were weighted to produce a data set with true oscillation parameters $\Delta m^2_{23} = 0.0025$ eV^2 and $\sin^2 2\theta_{23} = 1.0$. A χ^2 fit to the visible energy distribution of the events was then performed to estimate the uncertainties on the measurement of these parameters. The visible energy was estimated by the summed pulse height of the event, where a scaling factor of 6000 photoelectrons per GeV was applied. Systematic errors were incorporated by minimizing the value of χ^2 as a function of the systematic shift at each point in $\Delta m^2_{23}, \sin^2 2\theta_{23}$ space. A penalty factor was applied to the χ^2 based on how far the shift was from nominal (zero) and the estimated size of the systematic error in question. The systematic errors considered in this fit were:

- Neutrino energy scale : assumed 2% error
- overall flux normalization: assumed 2% error

- NC cross-section uncertainty : assumed 5% error

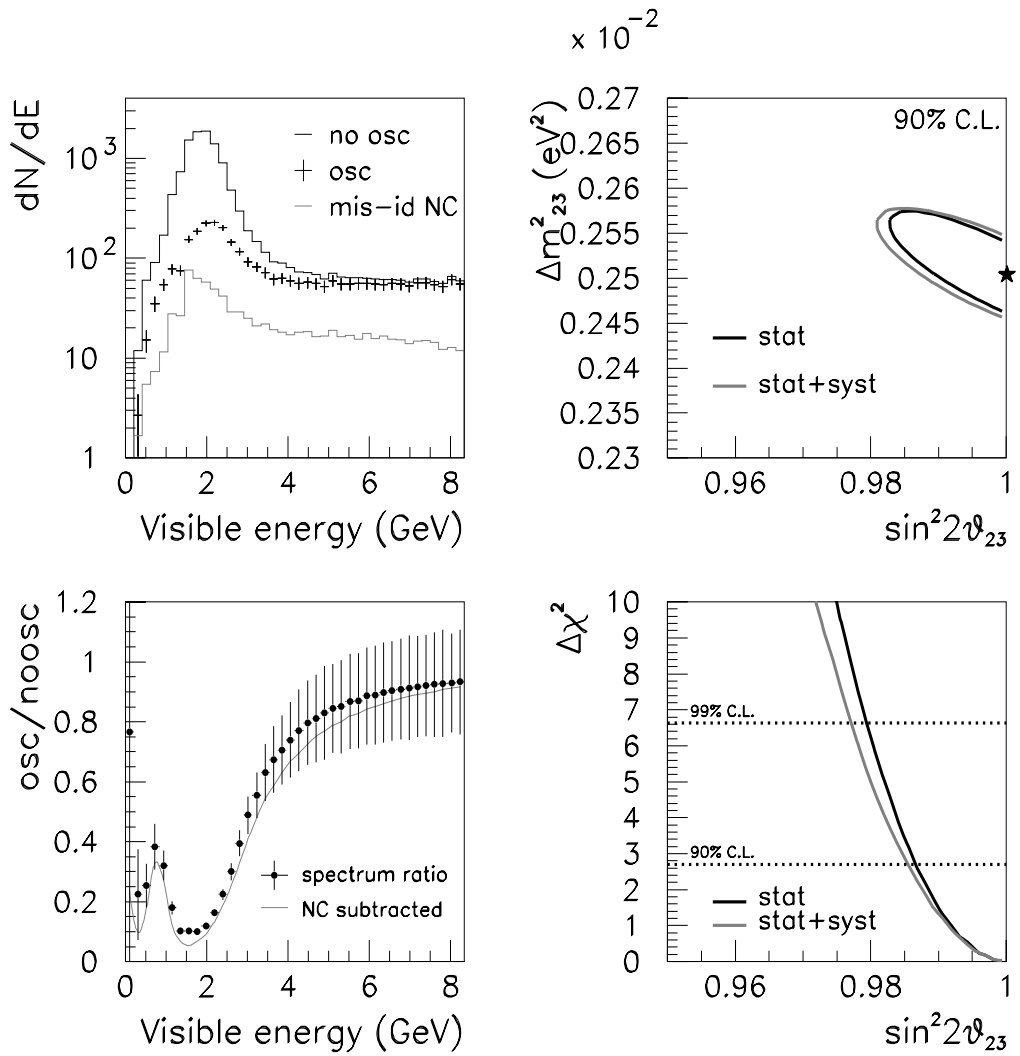

Figure 3: Results of a χ^2 fit to the visible energy spectrum of CC-like events, assuming true oscillation parameters $\Delta m^2_{23} = 0.0025$ eV^2 and $\sin^2 2\theta_{23} = 1.0$. An exposure of 250 kiloton years with a proton intensity of 3.7e20 p.o.t/yr. was assumed. See text for details.

Figure 3 shows the results of the fit. The plot at top-left shows (on a log scale) the visible energy spectrum of the unoscillated and oscillated true ν_μ CC events (black histogram and points respectively) and the contamination of mis-identified neutral current events (gray histogram). The bottom-left plot shows the ratio of the oscillated to unoscillated spectrum as a function of visible energy. The dip and low-energy rise in the spectrum ratio is clearly visible here. The gray line shows the ratio that is obtained if the neutral current background is subtracted - the effect of mis-identified NC events on the spectrum ratio is small, except at the lowest energies. The top-right plot shows the allowed region (90% C.L., 2 d.o.f.) obtained in $\Delta m^2_{23}, \sin^2 2\theta_{23}$ parameter space for statistical errors only (black contour) and

statistical and systematic errors combined (gray contour). The star denotes the values of the the input parameters. The bottom-right plot shows the $\Delta\chi^2$ distribution (1 d.o.f.) as a function of $\sin^2 2\theta_{23}$, where the value of χ^2 has been minimized with respect to Δm^2_{23}. The error on $\sin^2 2\theta_{23}$ (90% C.L., 1 d.o.f.) from this fit is approximately 1.5%. Figure 4 shows the improvement in the measurement of the parameters Δm^2_{23} and $\sin^2 2\theta_{23}$ that the off-axis experiment would provide over MINOS and the current Super-K allowed region. The off-axis and MINOS allowed regions are calculated assuming a 5 year exposure (3.7e20 p.o.t. per year) of each experiment.

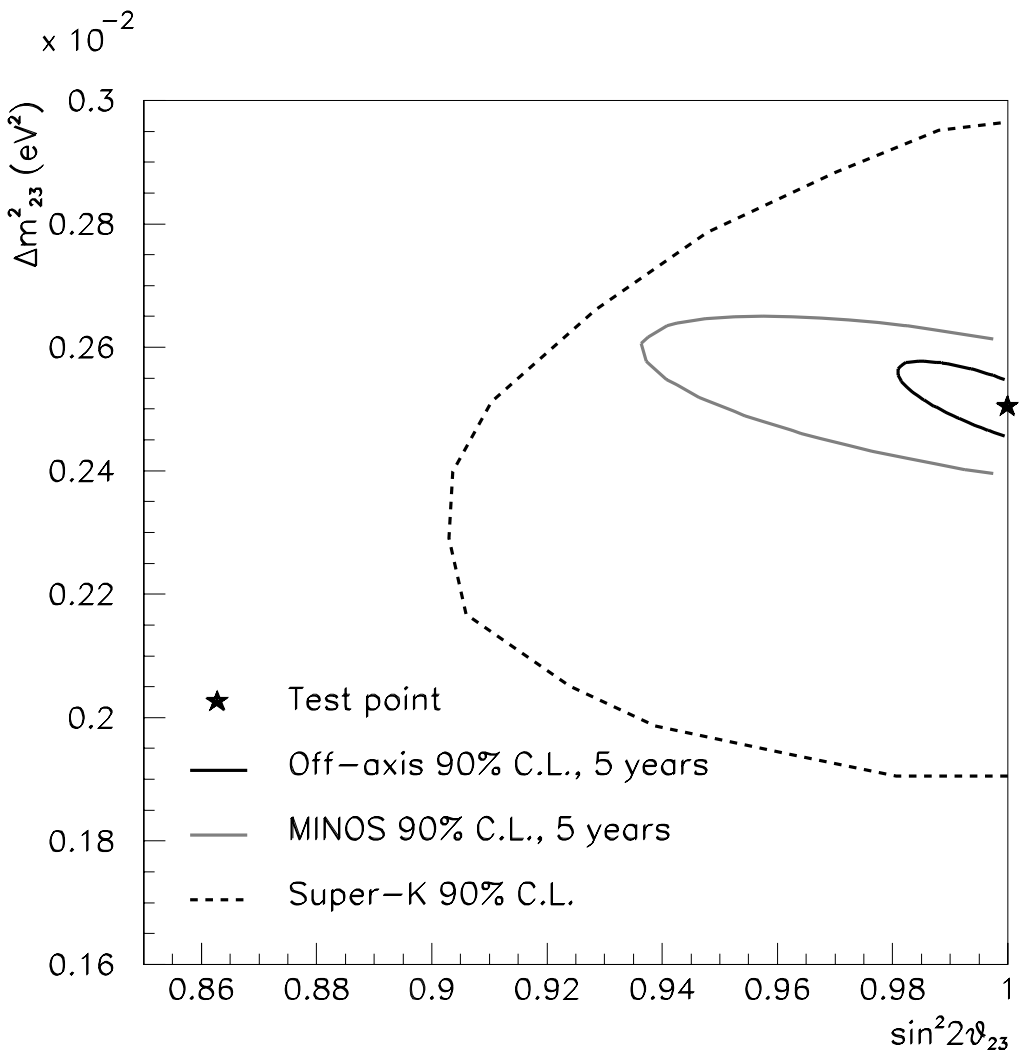

Figure 4: Comparison of measurement errors on the parameters $\Delta m^2_{23}, \sin^2\theta$ for the off-axis experiment and MINOS, assuming true parameters $\Delta m^2_{23} = 0.0025$ eV^2 and $\sin^2 2\theta_{23} = 1.0$. A 5 year exposure of each experiment is assumed, with 3.7e20 p.o.t per year. The current Super-K allowed region is also shown.

Figure 5 shows the results of a fit to an oscillation signal with a value of $\sin^2 2\theta_{23} < 1$. The parameters assumed were $\Delta m^2_{23} = 0.0025$ eV^2 and $\sin^2 2\theta_{23} = 0.95$, which is within the present Super-Kamiokande 90% C.L. atmospheric neutrino allowed region. The right-hand plot, which shows the $\Delta\chi^2$ distribution as a function of $\sin^2 2\theta_{23}$, indicates that, for this value of $\sin^2 2\theta_{23}$, it should be possible to exclude maximal mixing ($\sin^2 2\theta_{23} = 1.0$) at greater than 99% C.L. (1 d.o.f.)

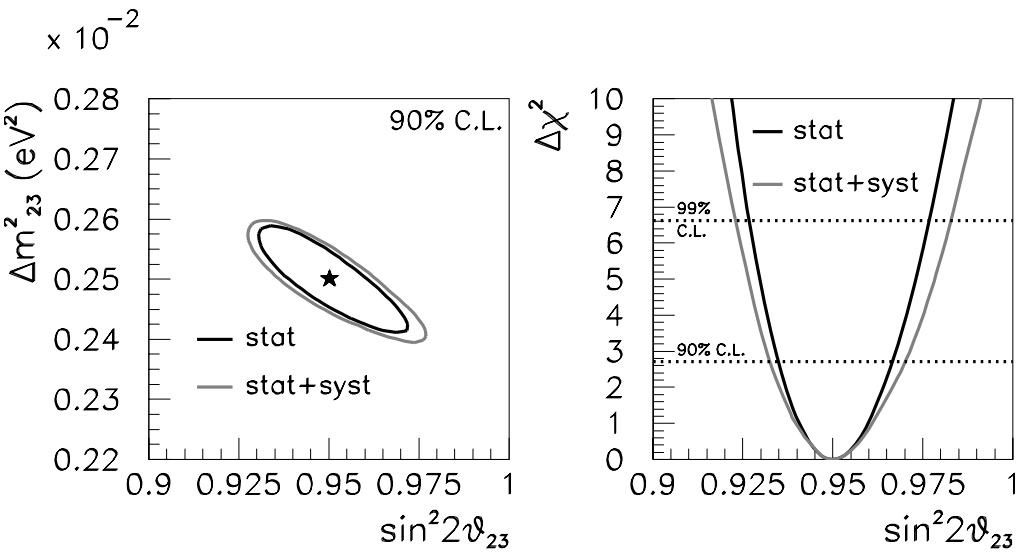

Figure 5: Measurement errors on the parameters $\Delta m^2_{23}, \sin^2\theta$ assuming true parameters $\Delta m^2_{23} = 0.0025$ eV^2 and $\sin^2 2\theta_{23} = 0.95$.

3 Limits on sterile neutrinos

The signature for $\nu_\mu \to \nu_s$ oscillations in the off-axis detector is a depletion of the number of observed neutral current events compared with the no-oscillation expectation. For this simulation, one additional parameter ($\sin^2 2\theta_{\mu s}$) was introduced which sets the amplitude of the $\nu_\mu \to \nu_s$ oscillations. It was assumed that the sum of active and sterile oscillation amplitudes was unity (maximal mixing) and that the active and sterile neutrinos oscillated with the same value of Δm^2.

The method used here to estimate the limit that could be set on $\sin^2 2\theta_{\mu s}$ in the absence of $\nu_\mu \to \nu_s$ oscillations is to isolate independent samples of NC-like and CC-like events and perform a simultaneous fit to the visible energy spectra. The NC-like sample is used to measure $\sin^2 2\theta_{\mu s}$ but has limited sensitivity to Δm^2, whereas the CC-like sample is used to measure Δm^2 but has little or no sensitivity to $\sin^2 2\theta_{\mu s}$.

The visible energy spectra for the CC-like and NC-like events samples are shown in figure 6. The approximate conversion factors between summed pulse height and visible energy are: 6000 pe/GeV for CC-like events and 4500 pe/GeV for NC-like events. The

plots show the visible energy distributions for three sets of parameter values: no oscillations (dashed histograms), pure active oscillations with $\Delta m^2 = 0.0025$, $\sin^2 2\theta_{23} = 1.0$ (gray histograms) and mixed active-sterile oscillations with $\Delta m^2 = 0.0025$ and $\sin^2 2\theta_{\mu s} = 0.15$ (black histograms). Note the suppression of the NC-like spectrum for the mixed active-sterile case. The shaded (green) histograms show the contribution of mis-identified wrong-flavor events in each sample. The rate of true ν_μ CC events that are mis-classified as NC-like is strongly suppressed by neutrino oscillations.

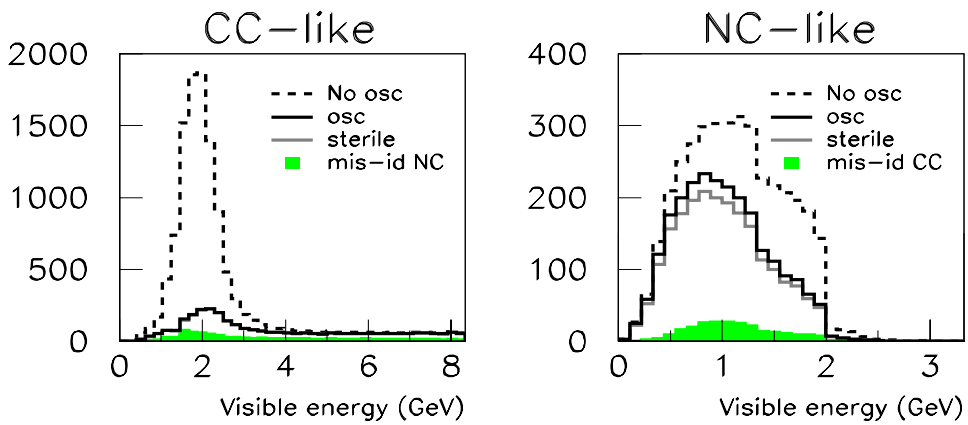

Figure 6: Visible energy distributions for CC-like and NC-like events. See text for details.

A simultaneous χ^2 fit to the visible energy spectra of both the CC-like and NC-like samples was performed to estimate the errors on the oscillation parameters $(\Delta m^2, \sin^2 2\theta_{\mu s})$. is assumed. The following systematic uncertainties were considered:

- Overall (correlated) flux uncertainty: 2% error.
- Energy scale uncertainty: 2% error.
- NC cross-section uncertainty: 2% error.

For each pair of parameters $(\Delta m^2, \sin^2 2\theta_{\mu s})$, the value of χ^2 was minimized with respect to these systematic uncertainties, and penalty factors were added to the χ^2 as these uncertainties deviated from their nominal values. Figure 7 shows the result of such a fit, where the true parameters are $(\Delta m^2 = 0.0025\ \mathrm{eV}^2, \sin^2 2\theta_{\mu s} = 0.0)$. The left-hand plot shows the allowed regions at 90 % C.L. in $\Delta m^2, \sin^2 2\theta_{\mu s}$ parameter space assuming statistical errors only (black contour) and statistical and systematic errors combined (gray contour). The right-hand plot shows $\Delta\chi^2$ as a function of $\sin^2 2\theta_{\mu s}$, where χ^2 has been minimized with respect to Δm^2. The figure shows that the limit (90% C.L., 1 d.o.f.) that could be set on the amplitude of $\nu_\mu \to \nu_s$ oscillations is approximately 5% assuming statistical errors only and 7% when systematic errors are also considered.

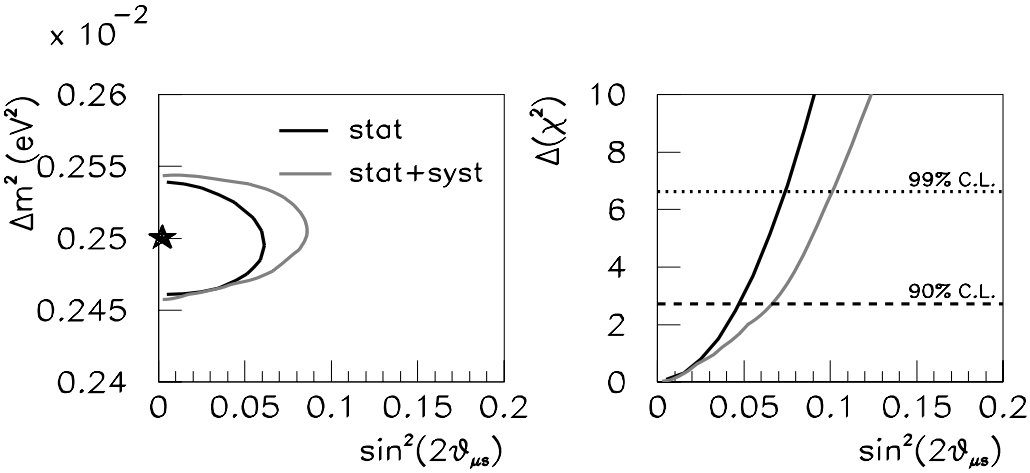

Figure 7: Allowed regions (90% C.L., 2 d.o.f.) in the $\Delta m^2, \sin^2 2\theta_{\mu s}$ plane from a fit to the visible energy distributions of CC-like and NC-like events, assuming statistical errors only (black contour) and also the systematic errors described in the text (gray contour). The simulated data were generated with oscillation parameters $\Delta m^2 = 0.0025$ eV^2 and $\sin^2 2\theta_{\mu s} = 0.0$. The plot at right shows the one-dimensional projection of the $\Delta\chi^2$ surface in the variable $\sin^2 2\theta_{\mu s}$.

A major systematic error associated with this analysis is the uncertainty in the the neutral current cross-section. At present, a conservative estimate of the uncertainty in the NC/CC cross-section ratio is $\sim$ 20% in the 1-10 GeV energy region. This is set to improve significantly in the next few years with measurements from K2K, MiniBoone and the MINOS near detector, and is likely to be known to an accuracy of 5% or better by the time the off-axis detector is operational. Figure 8 shows how uncertainties in the NC cross-section affect the measurement of $\sin^2 2\theta_{\mu s}$. It shows the $\Delta\chi^2$ distribution as a function of $\sin^2 2\theta_{\mu s}$, plotted for three values of the NC cross-section error, and indicates that the uncertainty on the NC rate should be less than 5% in order for a precision ($< 10\%$) measurement of the amplitude of $\nu_\mu \to \nu_s$ oscillations to be made.

4 Results for L=810 km and 10 km off-axis

The analyses described above have also been carried out for an off-axis detector located 810 km from the neutrino source and 10 km off-axis. Figure 9 shows the true CC energy spectrum at this location, compared to the spectrum at 12 km off-axis. The peak in the spectrum moves to higher energies and there is a $\sim$50% increase in the total event rate. However, the rate at the lowest energies ($\sim$2 GeV and below) is reduced.

As a result of the higher mean energy of the 10 km off-axis beam, the separation of charged-current and neutral current events is cleaner than for the 12 km off-axis case. Using the same cuts on the likelihood parameter as before, a CC selection efficiency of 83.7% is obtained, with a NC contamination of 6.9%. The corresponding numbers for

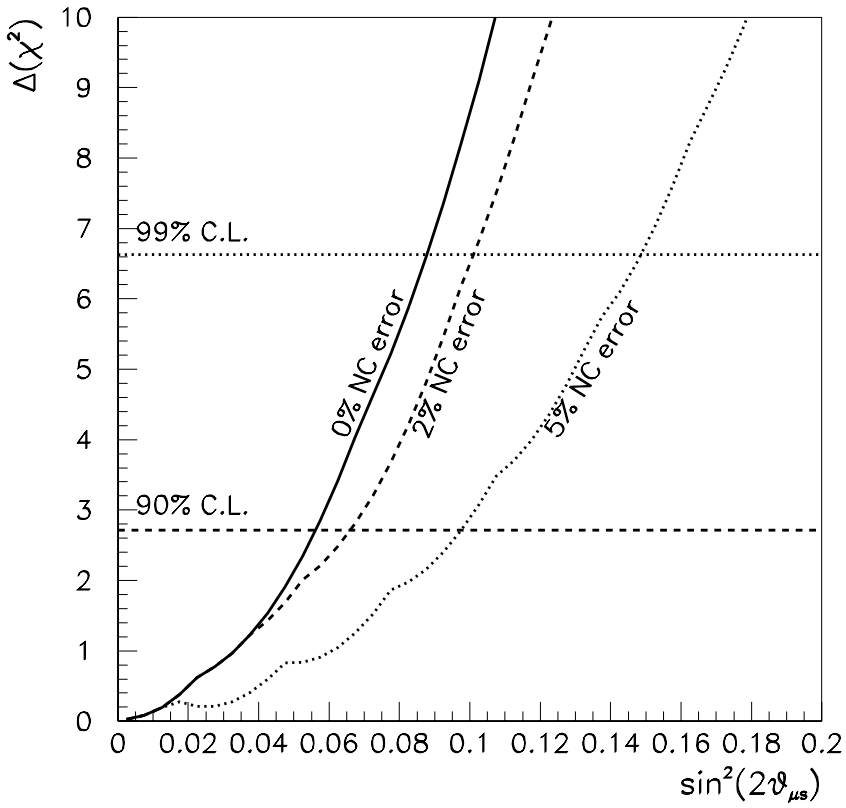

Figure 8: One-dimensional projection of the $\Delta\chi^2$ surface in the variable $\sin^2 2\theta_{\mu s}$ for fits assuming three values of the NC cross-section uncertainty. The simulated data were generated with oscillation parameters $\Delta m^2 = 0.0025$ eV^2 and $\sin^2 2\theta_{\mu s} = 0.0$.

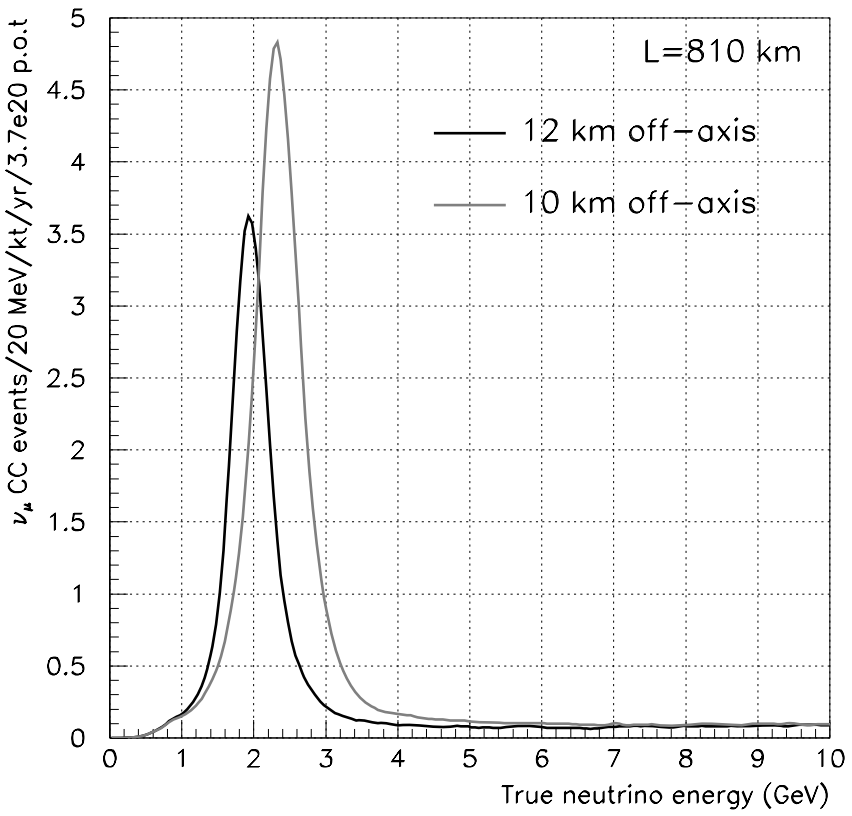

Figure 9: True ν_μ CC energy spectra at L=810 km and 10 and 12 km off-axis.

the 12 km off-axis beam are 82.4% and 7.4% respectively. The neutral current selection efficiency is 65.0% with a CC contamination of 37.5%. This compares to 57.9% and 42.0% for the 12 km off-axis beam.

Figure 10 shows the spectrum ratio and allowed regions from fits to a simulated oscillation signal with $\Delta m^2_{23} = 0.0025\,\mathrm{eV}^2$ and $\sin^2 2\theta_{23} = 1$. It can be seen that the measurement errors on the oscillation parameters are larger than for the 12 km off-axis case. Similarly, the result of fits to an oscillation signal with $\Delta m^2_{23} = 0.0025$ eV^2 and $\sin^2 2\theta_{23} = 0.95$ show a reduced potential to discriminate against $\sin^2 2\theta_{23} = 1.0$. In general, for a precise measurement of Δm^2_{23} and $\sin^2 2\theta_{23}$, it is desirable for the peak in the energy spectrum to lie at the first oscillation minimum and, for $\Delta m^2_{23} = 0.0025$ eV^2 and L=810 km, the first oscillation minimum occurs at 1.63 GeV. The 12 km off-axis beam, which peaks at around 1.9 GeV is therefore more favourable for a measurement of Δm^2_{23} and $\sin^2 2\theta_{23}$ than the 10 km off-axis beam, which peaks at around 2.3 GeV.

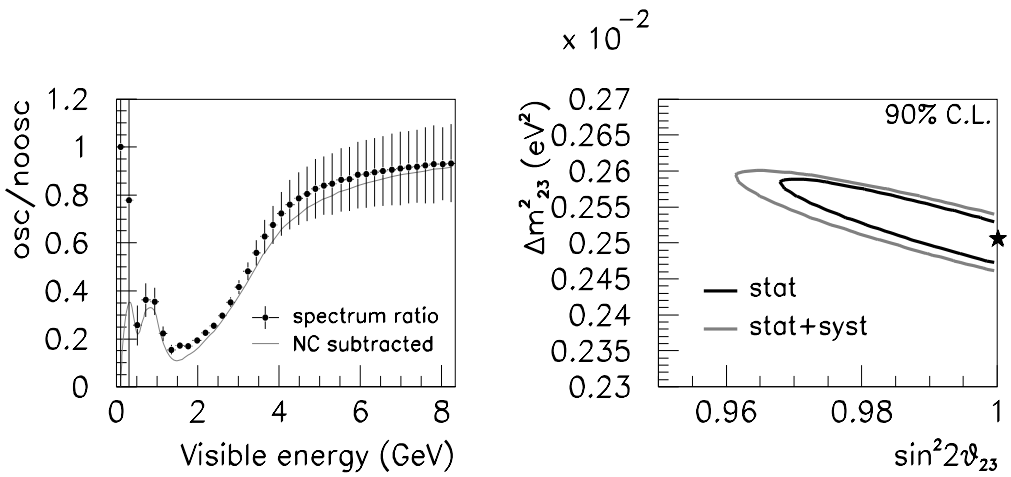

Figure 10: Spectrum ratio and allowed region in the $\Delta m^2, \sin^2 2\theta_{23}$ plane from a fit to the visible energy spectrum of CC-like events, assuming true oscillation parameters $\Delta m^2_{23} = 0.0025$ eV^2 and $\sin^2 2\theta_{23} = 1.0$. An exposure of 250 kiloton years of the 10 km off-axis beam with a proton intensity of 3.7e20 p.o.t/yr. was assumed.

The situation is reversed for the $\nu_\mu \to \nu_s$ measurement, as shown in figure 11. Here the 10 km off-axis beam produces a somewhat more restrictive limit on $\sin^2 2\theta_{\mu s}$ than the 12 km off-axis beam. This is due to the larger overall flux for the 10 km off-axis beam. The effect of shifting the peak of the energy spectrum away from the oscillation minimum is less pronounced here, as the neutral current events selected by the likelihood method tend to have high visible energy.

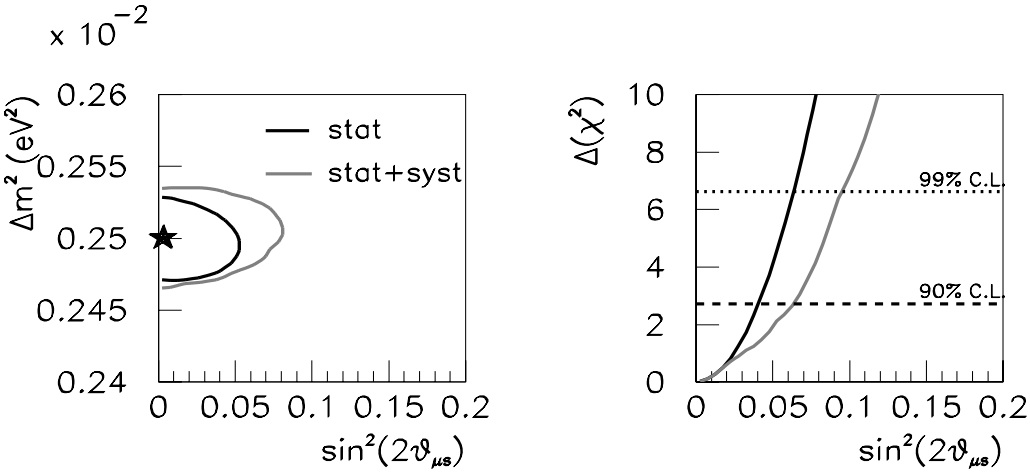

Figure 11: Allowed region in the $\Delta m^2, \sin^2 2\theta_{\mu s}$ plane and 1D projection in the variable $\sin^2 2\theta_{\mu s}$, assuming true oscillation parameters $\Delta m^2_{23} = 0.0025$ eV^2 and $\sin^2 2\theta_{\mu s} = 0.0$. An exposure of 250 kiloton years of the 10 km off-axis beam with a proton intensity of 3.7e20 p.o.t/yr. was assumed.

5 Summary and conclusions

The sensitivity of the scintillator-based off-axis detector to ν_μ disappearance and $\nu_\mu \to \nu_s$ signals has been investigated in this note. For the ν_μ disappearance measurement, it is possible to measure the parameters Δm^2_{23} and $\sin^2 2\theta_{23}$ to a precision of 2% or better, assuming true parameters $\Delta m^2_{23} = 0.0025$ eV^2 and $\sin^2 2\theta_{23} = 1$, and 2×10^{21} protons on target. A limit of approximately 7% can be set on the $\nu_\mu \to \nu_s$ amplitude from a combined fit to the identified CC-like and NC-like samples, although this limit depends strongly on the systematic errors assumed. This measurement is likely to be systematics limited until more precise measurements of CC and NC cross-sections in the 1-3 GeV region are made.

These sensitivities were calculated for the off-axis beam spectrum expected at a distance of 810 km from Fermilab and 12 km off-axis. They were repeated for $L = 810$ km and 10 km off-axis, which produces a beam with $\sim 50\%$ more flux and peaks at 2.3 GeV as opposed to 1.9 GeV for the 12 km case. Since the first oscillation minimum occurs at 1.6 GeV for the test point of $\Delta m^2_{23} = 0.0025$ eV^2, the measurement errors on parameters Δm^2_{23} and $\sin^2 2\theta_{23}$ are larger for the 10 km off-axis case, as the dip in the ν_μ CC spectrum is less well-resolved.

References

[1] Peter Litchfield, Leon Mualem, David Petyt, Simulation of a Solid Scintillator Off-axis Detector, Off-axis-Note-SIM-23.